Electronic supplementary information

$Ni_{1-2x}Mo_xSe$ nanowires@ammonium nickel phosphate—MoO_x hybrids as a high performance electrocatalyst for water splitting

Pianpian Zhang, Leibo Gong, and Yiwei Tan*

State Key Laboratory of Materials-Oriented Chemical Engineering, School of Chemistry and Chemical Engineering, Nanjing Tech University, Nanjing 211816, China, Email: ytan@njtech.edu.cn

Experimental section

Materials

Nickel(II) chloride hexahydrate ($NiCl_2·6H_2O$, Sigma-Aldrich, 99.9%), ammonium molybdate tetrahydrate ($(NH_4)_6Mo_7O_{24}·4H_2O$, Alfa Aesar, 99%), sodium molybdate dihydrate ($Na_2MoO_4·2H_2O$, Sigma-Aldrich, ≥99.5%), selenic acid (Alfa Aesar, H_2SeO_4, 40% aqueous solution), diammonium hydrogen phosphate ($(NH_4)_2HPO_4$, Alfa Aesar, 98%), 2,5-dimethoxyaniline (Alfa Aesar, 99%), trisodium citrate dihydrate ($Na_3(C_3H_5O_7)·2H_2O$, Sigma-Aldrich, ≥99.0%), N-methyl-2-pyrrolidinone (Alfa Aesar, >99%) were purchase form various commercial sources. A piece of Ni foam (NF) was cut into equal parts (1 cm × 3 cm) and sequentially pretreated with isopropanol, hydrochloric acid (0.1 M), and ethanol under ultrasonication to remove grease and the surface oxide layer. Ultrapure water (18.2 MΩ) produced with a Milli-Q purification system was used in the synthesis and electrochemical measurements.

Synthesis

Synthesis of high-density $Ni_{1-2x}Mo_xSe$ nanowire arrays on NF ($Ni_{1-2x}Mo_xSe$/NF). In a typical experiment, 2,5-dimethoxyaniline (0.1241 g, 0.810 mmol) and ammonium molybdate tetrahydrate (0.0883 g, 0.0714 mmol) were dissolved in a mixed solvent of pyridine (20 mL) and water (11.5 mL), and then mixed with 6.75 mL of an aqueous solution of selenic acid (0.08 M). Afterwards, the reaction solution was transferred into a 50 mL Teflon-lined stainless steel autoclave. After several (3−4) pieces of cleaned and dried NF were immersed into the autoclave containing the preceding precursor solution, the autoclave was sealed and maintained at 200 ºC for 20 h and then naturally cooled down to ambient temperature. The resulting $Ni_{1-2x}Mo_xSe$/NF electrodes were isolated by decanting the reaction solution, followed by rinsing 5 times alternately with water and N-methyl-2-pyrrolidinone at 50 °C to remove the adsorbed poly(2,5-dimethoxyaniline) from the $Ni_{1-2x}Mo_xSe$ nanowire surface, and dried at 60 °C in a vacuum oven for 5 h. The mass loading of $Ni_{1-2x}Mo_xSe$ nanowires on NF is 6.4 mg cm^{-2} based on the weighing analysis in combination with the reaction equation and its chemical composition.

The reference electrode preparation

For the preparation of Pt/C working electrode as a reference, 2 mg of Pt/C (20 wt% Pt) and 10 μL of Nafion solution (5 wt%) were dispersed in 1.0 mL of water/isopropanol (v/v = 4 : 1) and then sonicated for 30 min to form a homogenous ink dispersion. Afterwards, 0.5 mL of the dispersion was drop-casted on a piece of NF with an exposure area of 0.5 cm^2 to obtain a loading amount of 0.4 mg cm^{-2} for the electroactive Pt.

Characterization of materials

Scanning electron microscopy (SEM) images and SEM energy dispersive X-ray spectroscopy (EDX) were acquired

using a Hitachi S-4800 field-emission scanning electron microscope to investigate the morphology and near-surface composition of the catalysts, operating at an acceleration voltage of 5 kV. Transmission electron microscopy (TEM) images were obtained using an FEI Tecnai G2 Spirit Bio TWIN transmission electron microscope operating at an accelerating voltage of 100 kV. High-resolution TEM (HRTEM) and scanning TEM (STEM) micrographs, and STEM-EDX elemental maps were acquired using an FEI ETEM Titan G2 60-300 Cs-corrected scanning transmission electron microscope equipped with a spherical aberration corrector for the electron beam operating at 300 kV to probe the crystallographic structure and composition of samples. STEM images and STEM-EDX elemental maps were obtained in high-angle annular dark field (HAADF) mode to provide the bulk chemical composition of samples. The specimens for TEM observations were carefully scratched from the NF support and sonicated before dropping them onto 300 mesh carbon-coated copper grids. To analyze the surface composition and elemental oxidation states of electrode samples, X-ray photoelectron spectroscopy (XPS) measurements were carried out using a Kratos Axis Supra (Kratos Analytical) spectrometer at 15 kV and 10 mA with a hemispherical energy analyzer, employing a monochromated microfocused (300 × 700 μm^2) Al-Kα (hv = 1486.58 eV) X-ray source. Samples for XPS measurements were sputtered by repeated cycles of Ar^+ ions to obtain clean electrode surfaces. The binding energies (BEs) of the core levels were calibrated by setting the adventitious C 1s peak at 284.8 eV. Survey spectra of the samples in the BE range of 0–1000 eV and the core level spectra of the elemental signals were collected with a step size of 1 and 0.1 eV, respectively. To obtain the phase and structure of samples, the X-ray diffraction (XRD) patterns were recorded using a Rigaku SmartLab diffractometer with a Cu Kα X-ray source (λ = 1.5406 Å, generated at 40 kV and 100 mA) at a scanning rate of 0.06° s^{-1}, and scanned in the Bragg–Brentano mode from 2θ of 10° to 90° in 0.02° increments. The $Ni_{1-2x}Mo_xSe$ nanowires carefully scratched from the NF support or the integrated electrodes were used as the specimen for XRD characterization after cleaning treatment. The chemical composition of the catalyst was determined by EDX quantitative analysis and/or inductively coupled plasma atomic emission spectrometry (ICP-AES, Prodigy, Leeman Labs Inc., λ = 165–800 nm, As = 200 nm) measurements after dissolving the sample in aqua regia.

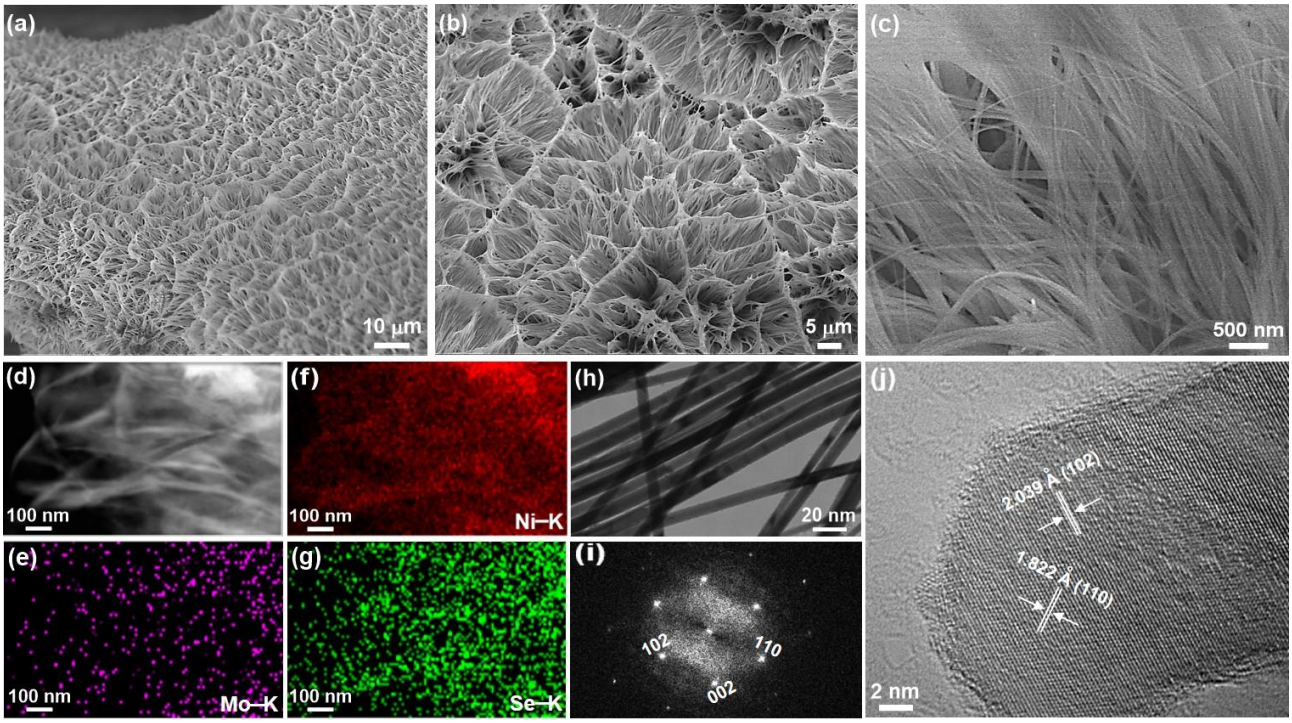

Figure S1. (a) Low-, (b) medium-, and (b) high-magnification SEM images of $Ni_{1-2x}Mo_xSe$ nanowire arrays on NF. (d) HAADF-STEM, (e–g) corresponding HAADF-STEM-EDX elemental mapping, (h) TEM, and (j) HRTEM images of $Ni_{1-2x}Mo_xSe$ nanowires. (i) The corresponding SAED pattern of the $Ni_{1-2x}Mo_xSe$ nanowire in panel (j).

The $Ni_{1-2x}Mo_xSe$/NF electrodes were produced *via* a facile solvothermal route, where the in-situ produced Se was directly reacted with the surface Ni atoms of NF that was used as the Ni source and with Mo^{4+} generated from the reduction of $(NH_4)_6Mo_7O_{24}\cdot 4H_2O$ used as the Mo source. In the synthesis, H_2SeO_4 and $Mo_7O_{24}^{6-}$ were first reduced by 2,5-dimethoxyaniline to form elemental Se and Mo(IV), and then, as a result, the product poly(2,5-dimethoxyaniline) formed after the oxidative polymerization acts as an in-situ capping agent to dictate the one-dimensional growth of the $Ni_{1-2x}Mo_xSe$ nanowires (see Fig. 1 in the text). The morphological and structural characterization shown in Figure S1 reveals the hierarchical $Ni_{1-2x}Mo_xSe$ nano-architecture grown on NF after the solvothermal reaction. Figure S1a–c exhibit the SEM images of $Ni_{1-2x}Mo_xSe$/NF at different magnifications. The overview SEM image in Figure S1a displays that the skeletal surface of NF is evenly and densely covered with $Ni_{1-2x}Mo_xSe$ nanowires that grow vertically from the NF substrate and self-assemble into a rippled sea of wheat-like superstructure, as clearly evidenced by the image of these nanowires at a high magnification (Figure S1b). A close-up examination of the superstructure reveals that numerous nanowires align in a certain direction and closely pack into long strands with a length of tens of micrometers (Figure S1c). Apparently, the $Ni_{1-2x}Mo_xSe$ nanowire superstructure in radial patterns and with rich porosity effectively boosts the contact area between the nanowires and the deposition bath and is beneficial to the densely coating of a secondary composite phase onto the nanowire surface. As demonstrated in the HAADF-STEM image and the corresponding HAADF-STEM-EDX elemental mapping images in Figure S1d–g, Ni, Mo, and Se are homogeneously distributed over the observed area. The intensity of Mo is significantly weaker than those of other elements, being indicative of its lower content in the sample. The corresponding STEM-EDX spectrum also confirms that the nanowires are composed of Ni, Mo, and Se (Figure S2a). The average chemical composition of $Ni_{1-2x}Mo_xSe$ nanowires is determined by the STEM-EDX quantitative analysis of the nanowires scratched from $Ni_{1-2x}Mo_xSe$/NF, which gives a bulk Ni/Mo/Se atomic ratio of 46.7 : 5.1 : 48.2. Simultaneously, the quantitative ICP-OES analyses present an average Ni/Mo/Se atomic ratio of 45.6 : 4.7 : 49.7, which closely matches

the above result.

The TEM image in Figure S1h further illustrates that the $Ni_{1-x}Mo_xSe$ nanowires are unform in diameter and have an average diameter of 18.5 nm. Representatively, the HRTEM image and the corresponding selected area electron diffraction (SAED) pattern in Figure S1j and S1i, respectively, are utilized to evaluate the crystalline structure of the as-synthesized $Ni_{1-2x}Mo_xSe$ nanowires. The well-resolved, continuous, parallel lattice fringes with a measured interplanar spacing of 2.039 and 2.822 Å, which can be tentatively assigned to the (102) and (110) lattice planes of the hexagonal $Ni_{1-2x}Mo_xSe$ structure, respectively, and the different consistent orientations in the HRTEM image confirm that the entire $Ni_{1-2x}Mo_xSe$ nanowires are single-crystalline. Moreover, the corresponding SAED pattern shows a set of regular, discrete diffraction spots, revealing the single crystalline nature of the $Ni_{1-2x}Mo_xSe$ nanowires (Figure S1i). The structure of the $Ni_{1-2x}Mo_xSe$ nanowires is further analyzed through the X-ray diffraction (XRD) pattern in Figure S3, in which all the diffraction peaks are analogous to the NiSe reference (JCPDF no. 65-9451, $a = b = 3.658$ Å and $c = 5.354$ Å) and can be perfectly indexed to the hexagonal sederholmite phase with the $P63/mmc$ space group. Meanwhile, all the Bragg peaks are shifted to higher angles relative to their counterparts of the NiSe reference, suggesting a fraction of Ni ions in NiSe lattices being substituted by the smaller Mo^{4+} ions (also see Fig. S6, ESI† and the corresponding discussions in the text). No additional peaks from other phases can be found, indicating that product is a single pure sederholmite phase. The unit cell parameters of the $Ni_{1-2x}Mo_xSe$ are calculated to be $a = b = 3.625$ Å and $c = 5.314$ Å.

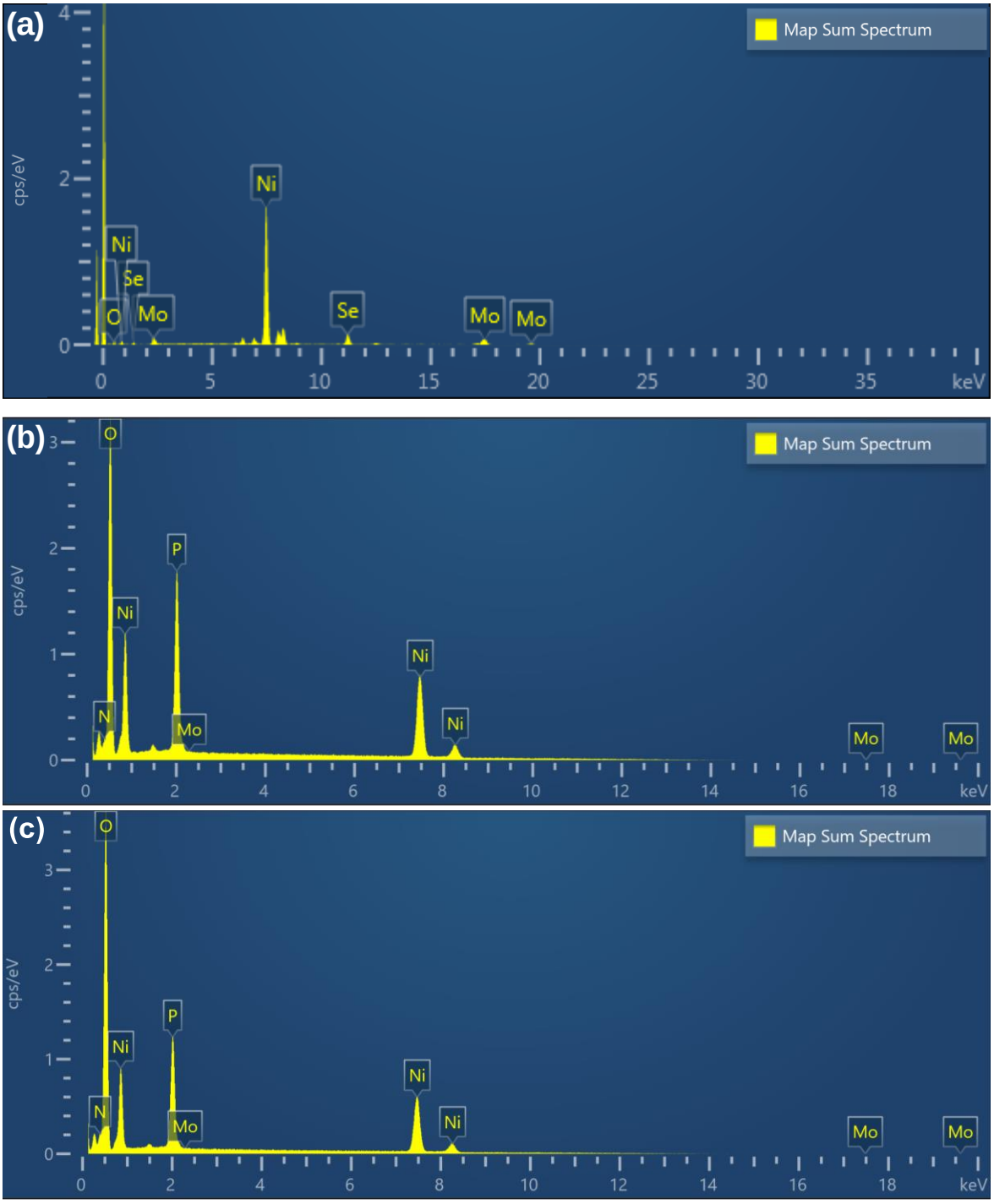

Figure S2. SEM-EDX spectra of (a) $Ni_{1-2x}Mo_xSe$/NF, (b) $Ni_{1-2x}Mo_xSe$@$NH_4NiPO_4·6H_2O$–MoO_x/NF, and (c) $NH_4NiPO_4·6H_2O$–MoO_x/NF.

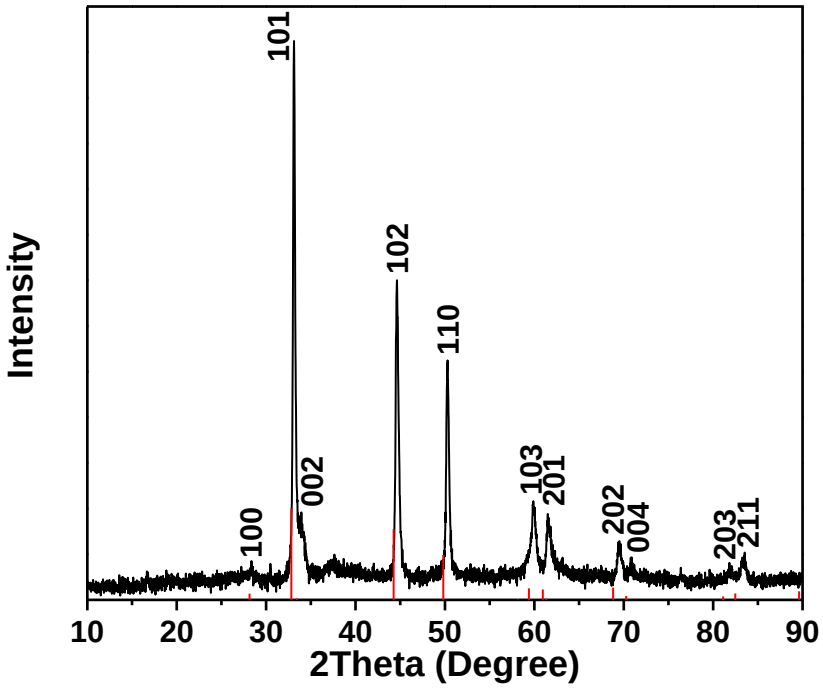

Figure S3. Powder XRD pattern of the as-prepared $Ni_{1-2x}Mo_xSe$ nanowires. For comparison, the intensities and positions for the pure NiSe reference indicated by the red bars are given at the bottom based on the JCPDS database (JCPDF no. 65-9451).

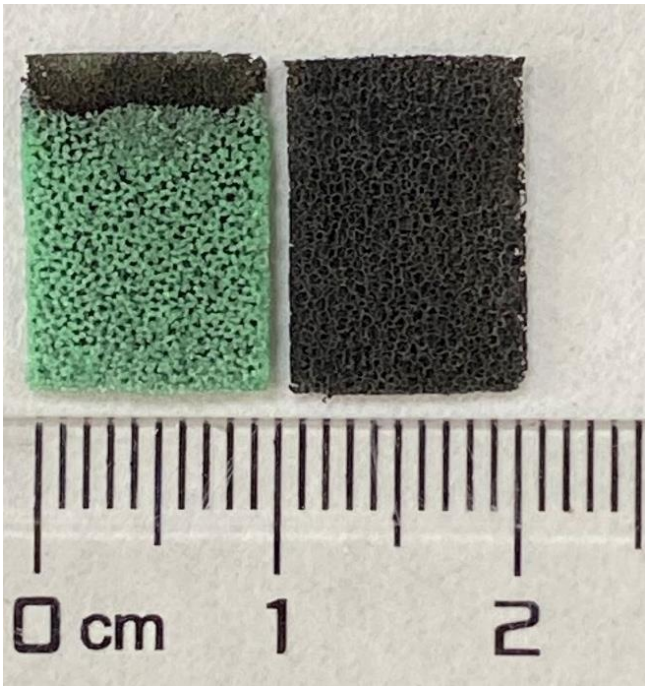

Figure S4. A digital photograph comparing a piece of $Ni_{1-2x}Mo_xSe@NH_4NiPO_4·6H_2O-MoO_x$/NF electrode (left) and a piece of $Ni_{1-2x}Mo_xSe$/NF electrode (right).

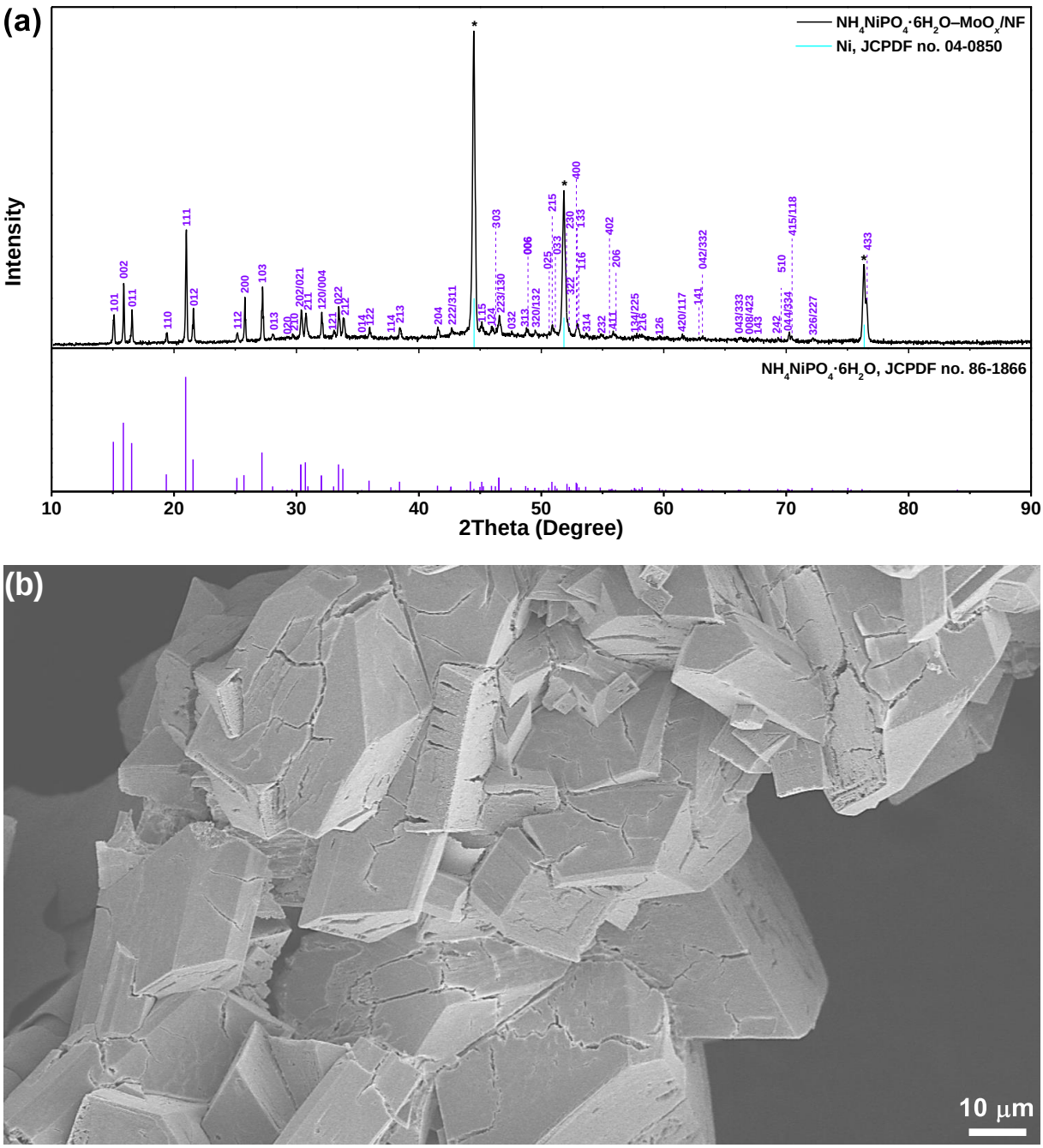

Figure S5. (a) XRD pattern and (b) SEM image of the $NH_4NiPO_4·6H_2O$–MoO_x/NF electrode. The peaks marked by an asterisk arise from the NF substrate. For comparison, the intensities and positions for the pure Ni and $NH_4NiPO_4·6H_2O$ references indicated by the cyan and magenta bars, respectively, are given at the bottom according to the JCPDS database (JCPDF no. 04-0850 and no. 86-1866).

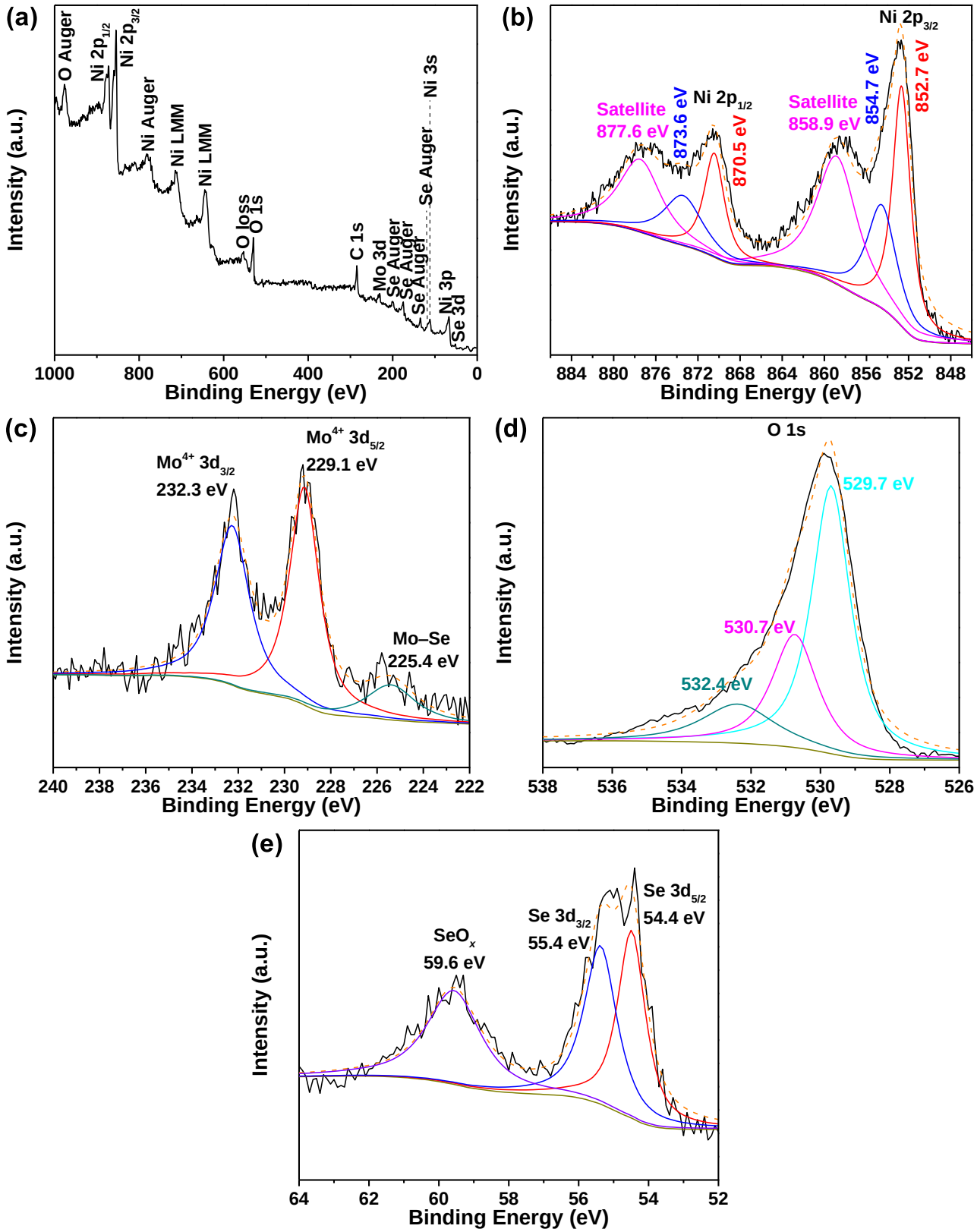

Figure S6. XPS characterization of the $Ni_{1-2x}Mo_xSe$/NF electrode. (a) XPS survey spectrum, (b) Ni 2p, (c) Mo 3d, (d) O 1s, and (e) Se 3d core-level spectra.

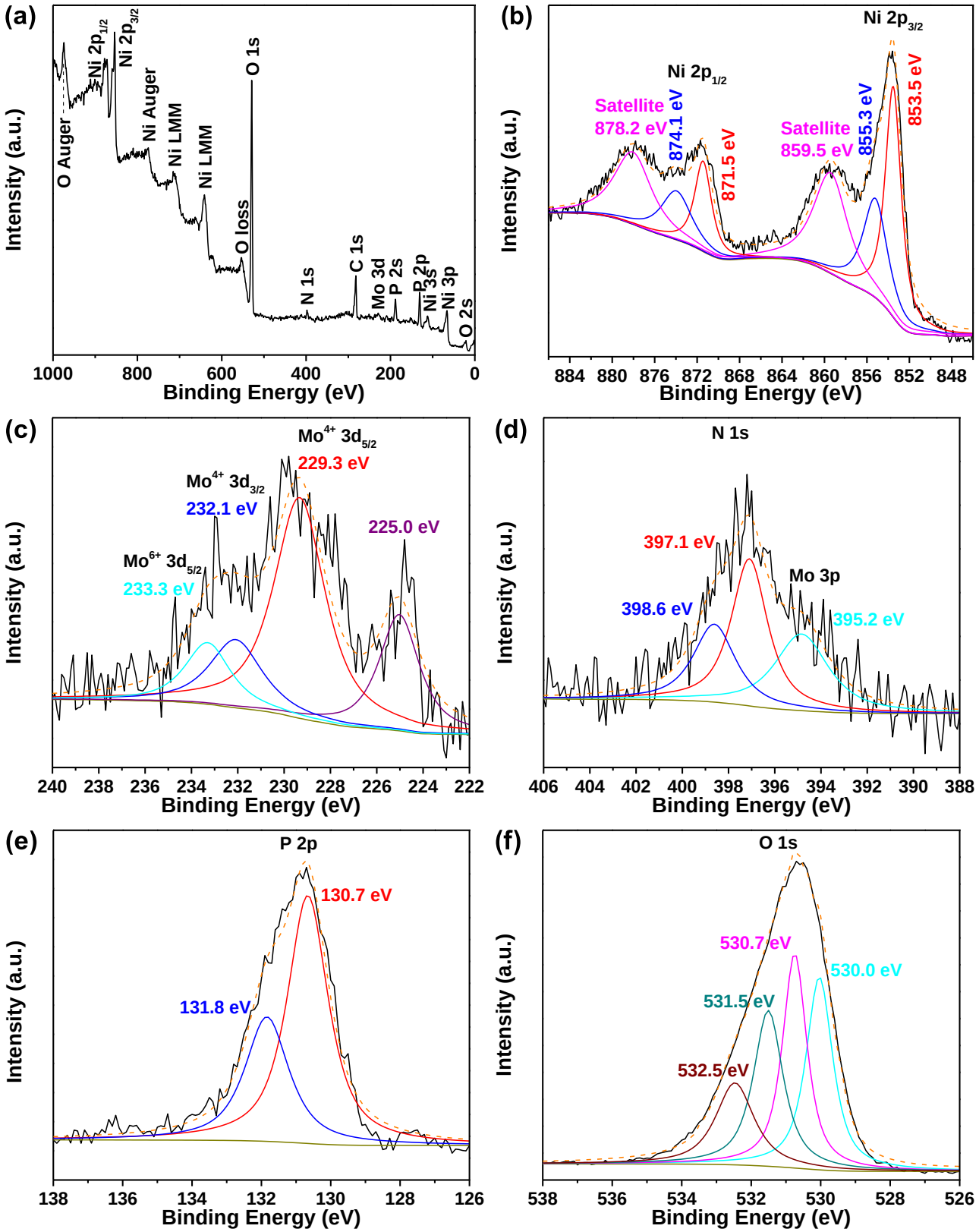

Figure S7. XPS characterization of the $NH_4NiPO_4 \cdot 6H_2O$–MoO_x/NF electrode. (a) XPS survey spectrum, (b) Ni 2p, (c) Mo 3d, (d) N 1s, (e) P 2p, and (f) O 1s core-level spectra.

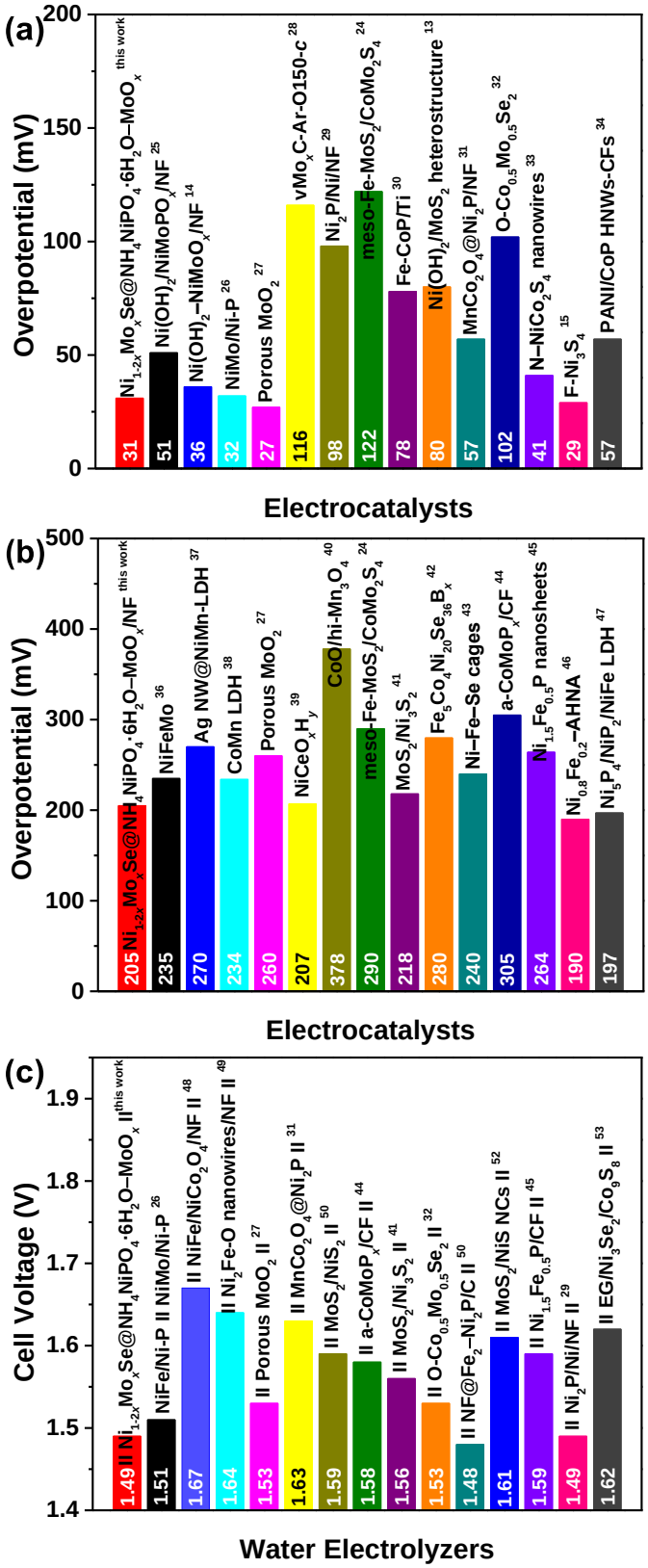

Figure S8. Comparison of the electrocatalytic activity of the previously reported catalysts in the literature with our ‖$Ni_{1-2x}Mo_xSe$@$NH_4NiPO_4·6H_2O$−MoO_x/NF‖ in this work. (a and b) The overpotentials required to attain the current density of (a) −10 mA cm^{-2} in the HER and (b) 10 mA cm^{-2} in the OER. (c) The cell voltage in overall water electrolyzer to achieve the current density of 10 mA cm^{-2}. All the data are collected in 1 M KOH. The references are given in the text.

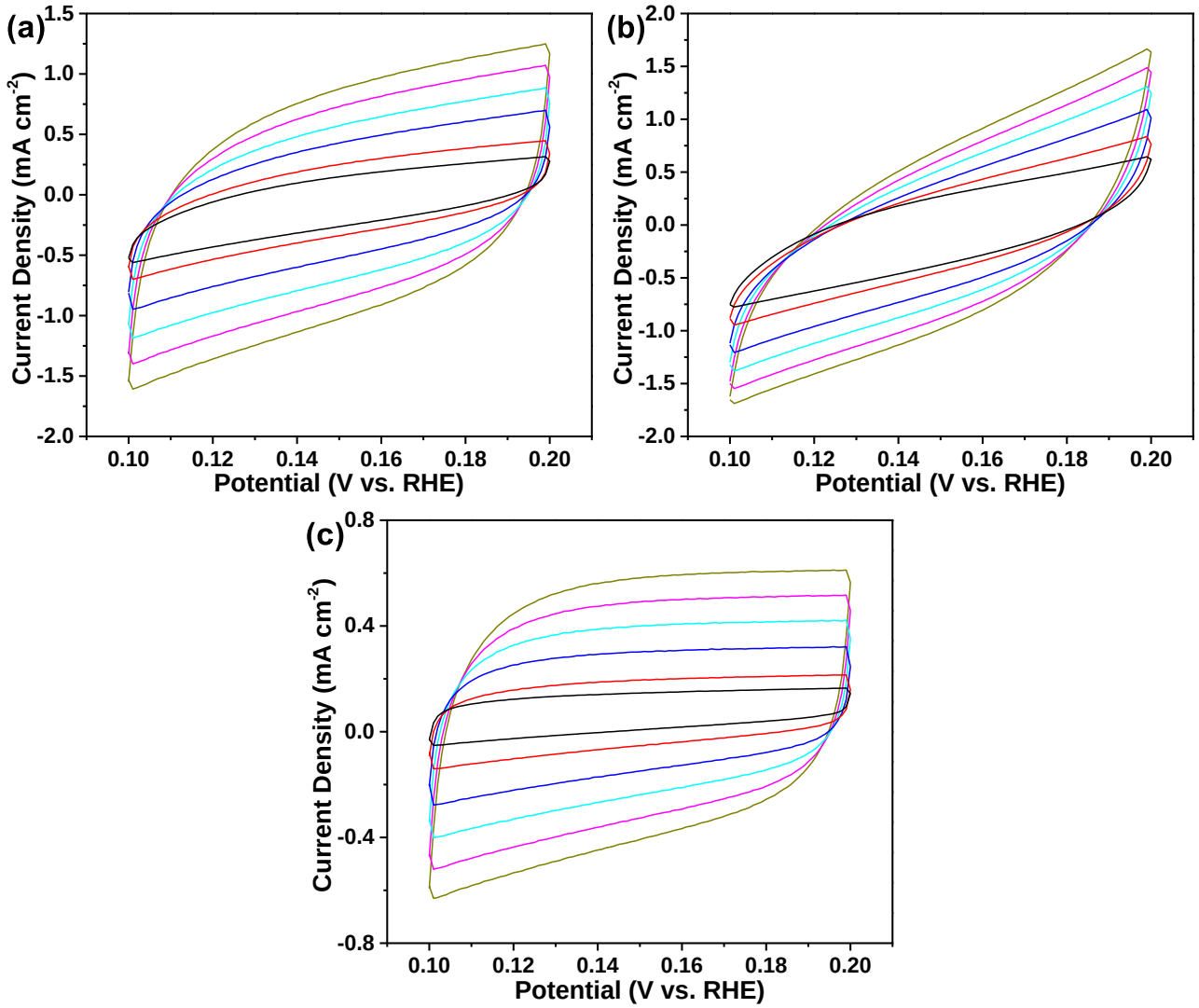

Figure S9. CV curves of (a) $Ni_{1-2x}Mo_xSe$@$NH_4NiPO_4 \cdot 6H_2O$−MoO_x/NF, (b) $NH_4NiPO_4 \cdot 6H_2O$−MoO_x/NF, and (c) $Ni_{1-2x}Mo_xSe$/NF. Scan rates of 5, 10, 20, 30, 40, and 50 mV s^{-1} were chosen.

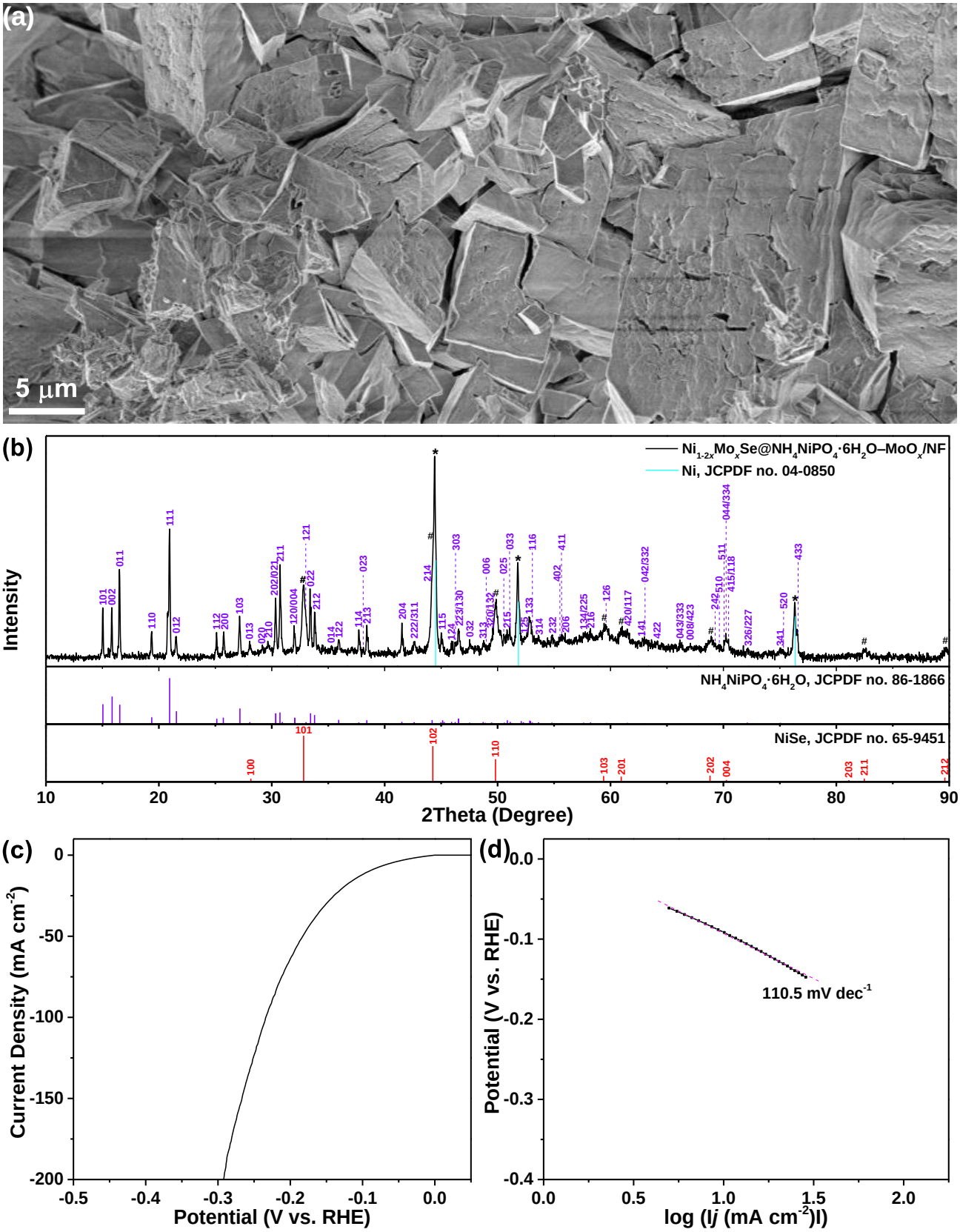

Figure S10. (a) SEM image, (b) XRD pattern, (c) polarization curve of the HER, and (d) Tafel plot of $Ni_{1-2x}Mo_xSe@NH_4NiPO_4{\cdot}6H_2O/NF$. The peaks marked by an asterisk or octothorp in panel (b) originate from NF or $Ni_{1-2x}Mo_xSe$ nanowires, respectively. For comparison, the intensities and positions for the pure Ni, NiSe, and $NH_4NiPO_4{\cdot}6H_2O$ references indicated by the cyan, red, and violet bars, respectively, are provided at the bottom of each panel of part (b) based on the JCPDS database (JCPDF no. 04-0850, no. 65-9451, and no. 86-1866).

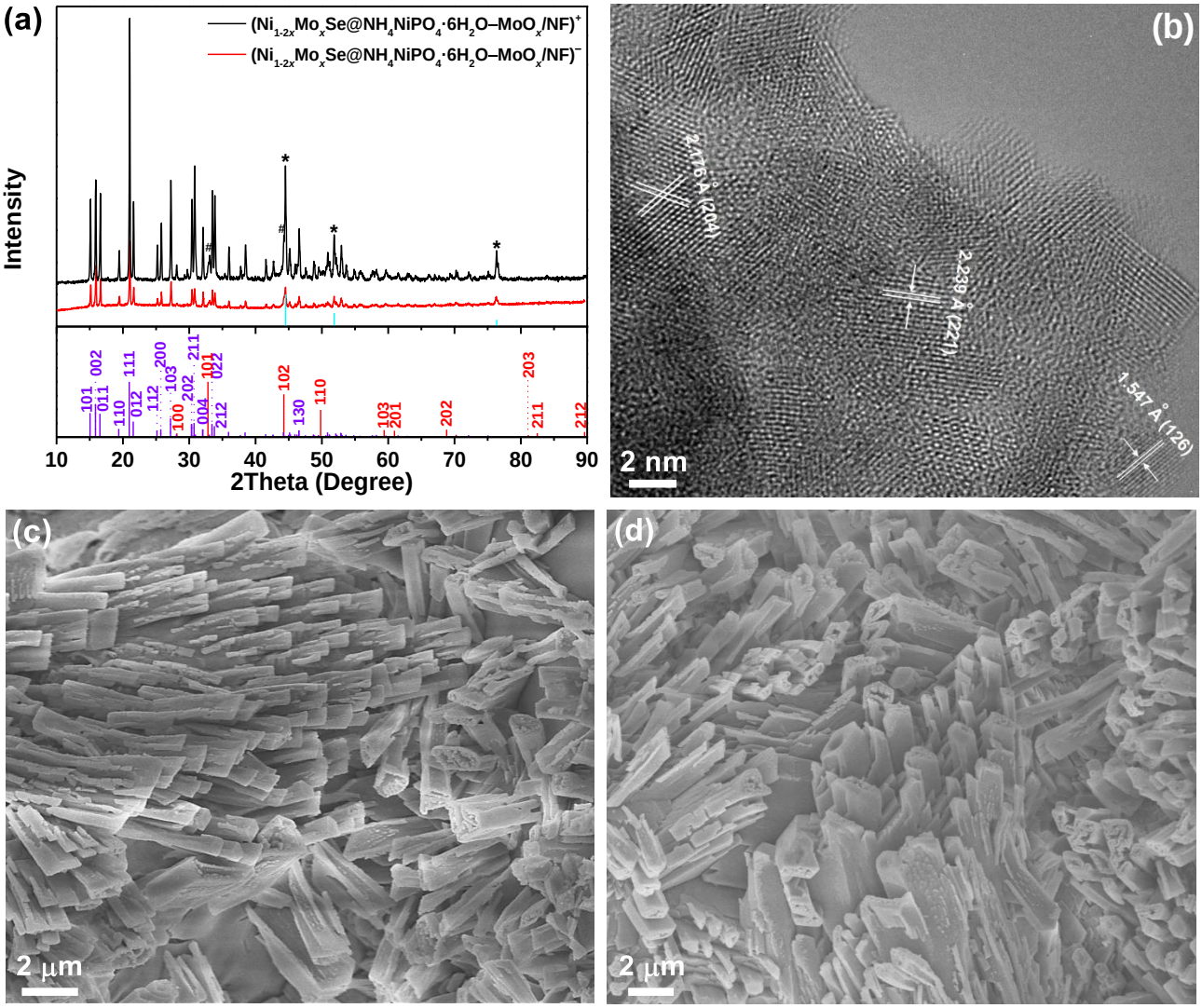

Figure S11. (a) XRD patterns, (b) HRTEM image, (c and d) SEM images of the (a, b, and c) $(Ni_{1-2x}Mo_xSe@NH_4NiPO_4{\cdot}6H_2O/NF)^+$ and (a and d) $(Ni_{1-2x}Mo_xSe@NH_4NiPO_4{\cdot}6H_2O/NF)^-$ obtained after CP measurement at a current density of 50 mA cm^{-2} for the overall-water-splitting over a period of 200 h in 1 M KOH. The peaks marked by an asterisk or octothorp in panel (a) arise from NF or $Ni_{1-2x}Mo_xSe$ nanowires, respectively. For comparison, the intensities and positions for the pure Ni, NiSe, and $NH_4NiPO_4{\cdot}6H_2O$ references indicated by the cyan, red, and violet bars, respectively, are given at the bottom of each panel of part (a) based on the JCPDS database (JCPDF no. 04-0850, no. 65-9451, and no. 86-1866). The well-defined lattice fringes with *d*-spacings of 2.176, 2.239, and 1.547 Å correspond well to the (204), (221), and (126) planes of $NH_4NiPO_4{\cdot}6H_2O$, respectively.